Deformation Bands and the Formation of Grain Boundaries in a Superplastic Aluminum Alloy

T.R. McNELLEY, D.L. SWISHER, and M.T. PÉREZ-PRADO

Superplastic aluminum alloys are often classified according to the mechanism of microstructural transformation during annealing after deformation processing. In Al-Cu-Zr materials, such as Supral 2004, the presence of fine (10 to 50 nm) second-phase particles retards dislocation rearrangement and the formation and migration of boundaries during either annealing or elevated temperature deformation after thermomechanical processing. This leads to predominance of recovery in the evolution of microstructure, although high-angle boundaries must still form in order to account for the superplastic response of such materials. The mechanisms of high-angle boundary formation in such circumstances have remained unclear. The term "continuous recrystallization" (CRX) has been used as a phenomenological description of recovery-dominated processes that take place uniformly throughout the microstructure and lead to the formation of fine grains with high-angle boundaries. Orientation imaging microscopy (OIM) methods have been employed to assess the as-processed microstructure of this alloy and its evolution during annealing at 450 °C, as well as during superplastic deformation at this temperature. Orientation images demonstrate the presence of deformation bands of alternating lattice orientations that corresponds to the symmetric variants of the brass, or B, texture component ($\langle 112\rangle\{110\}$ in rolled material). During annealing, the high-angle grain boundaries (disorientation of 50 to 62.8 deg) develop from transition regions between such bands while the lower-angle boundaries (*i.e.*, up to 20 deg) separate an evolving cell structure within the bands. Further OIM results show that the bands remain distinct features of the microstructure during either annealing alone or during deformation under superplastic conditions.

I. INTRODUCTION

HIGHLY refined and stable grain sizes and grain boundaries that resist tensile separation during elevated temperature deformation are required for superplasticity. In wrought aluminum alloys, grain refinement for superplasticity can only be achieved by deformation and recrystallization. However, our current understanding of deformation-induced microstructures in aluminum alloys is incomplete, and our knowledge of recrystallization is mainly empirical in nature.[1] At least two distinct thermomechanical processing (TMP) routes have been developed to enable superplastic response in aluminum alloys. The current understanding of the microstructural transformations associated with such TMPs has recently been reviewed.[2,3] The process of interest in the present work involves the continuous recrystallization (CRX) reaction in Supral 2004.[4,5] For as-cast material, the TMP consists of severe deformation by hot and cold rolling under conditions that allow the retention of fine second-phase particles of the Al_3Zr phase. These particles hinder dislocation rearrangement and the formation and migration of boundaries, thereby leading to a predominance of recovery in the CRX reaction.[6] Materials that undergo CRX, such as Supral 2004, generally retain well-defined deformation textures and develop bimodal disorientation distributions.[7,8,9] The term "disorientation" refers to the *minimum* angle among all crystallographically equivalent rotations relating the lattices of *adjacent* grains.

In a recent investigation of CRX in a superplastic Al-Ca-Zn alloy, the presence of grain clusters having lattice orientations corresponding to the symmetric variants of a copper, or C, type texture component ($\{112\}\langle 111\rangle$) has been documented.[3] The CRX reaction during static annealing included the development of distinct boundaries accompanied by the retention and sharpening of the texture and development of a bimodal distribution of boundary disorientation angles. The high-angle boundaries (50 to 62.8 deg) in the distribution were apparently the interfaces between the grain clusters, while the lower-angle boundaries (2 to 15 deg) corresponded to a cellular substructure within the clusters. It was suggested that the grain clusters and, therefore, the high-angle boundaries might have formed as a result of deformation banding (DB) during the severe warm and cold rolling of the TMP.[3]

A mechanism of grain subdivision, DB may start at the initiation of and continue throughout large-strain plastic deformation. As a consequence of this process, adjacent regions of a grain experience lattice rotation towards symmetrically related final orientations. These regions, or zones, of different lattice orientation become ribbonlike in shape during rolling deformation and have been termed "deformation bands." The existence of DB was suggested as early as 1940 by Barrett[10] and Barrett and Levenson.[11] Chin and Wonsiewicz[12] have also emphasized the importance of DB.

T.R. McNELLEY, Professor and Chairman, and D.L. SWISHER, Graduate Student, are with the Department of Mechanical Engineering, Naval Postgraduate School, Monterey, CA 93943-5146. M.T. PÉREZ-PRADO, Research Scientist, Centro Nacional de Investigaciones Metalurgicas (CENIM), 28040 Madrid, Spain, is Assistant Project Scientist, Department of Mechanical and Aerospace Engineering, University of California-San Diego, La Jolla, CA 92093-0411.

This article is based on a presentation made in the workshop entitled "Mechanisms of Elevated Temperature Plasticity and Fracture," which was held June 27–29, 2001, in San Diego, CA, concurrent with the 2001 Joint Applied Mechanics and Materials Summer Conference. The workshop was sponsored by Basic Energy Sciences of the United States Department of Energy.

Duggan and co-workers[13–18] have recently investigated the nature and origin of DB in polycrystalline fcc metals. According to these authors, the occurrence of this phenomenon is dependent on the initial grain size, and it predominates mainly in coarse-grained materials. The initial grain orientation and rolling reduction are also factors,[13] and DB can commence either at the onset of plastic deformation or at some larger strain. Banding is favored by the simultaneous occurrence of dynamic recovery, which enables the rearrangement of the dislocations in the band interiors into low energy arrays, thereby reducing the stored energy.[14]

Compatible deformation under plane strain conditions for a structure of elongated deformation bands may occur with the activation of only two slip systems in each band due to the relaxation of constraints.[15,19,20] The Taylor model[21] requires the operation of at least five independent slip systems for compatible deformation of a polycrystalline material composed of equiaxed grains having random lattice orientations. In a banded structure, there may be less strain hardening due to dislocation entanglement because there are fewer operative slip systems and, therefore, a lower flow stress since less work is done. In order for DB to be energetically favorable, this decrease in plastic work during straining must exceed the additional energy required for the creation of the band interfaces plus the accommodation of shears at the band ends.[15]

As pointed out recently by Kulkarni *et al.*,[22] "this phenomenon still remains remarkably enigmatic" despite the publication in recent years of several studies on DB in a variety of different materials.[23–42] Experimental evidence for DB has been reported mainly in studies of pure metals and also in dispersion hardened materials.[23–37] Detailed studies of the role of DB in high solute content materials are lacking, and the role of DB in the development of grain boundaries during CRX has not been addressed.

In the following section, the importance of grain refinement and the need for development of high-angle boundaries in order to enable superplasticity will be reviewed. Subsequently, orientation imaging microscopy (OIM) data will be presented that demonstrates the presence of deformation bands in as-processed, processed, and annealed Supral 2004. The high-angle boundaries that support superplasticity in this material will be shown to form as the interfaces between bands having lattice orientations corresponding to the symmetric variants of the main texture component. This work provides support for the role of DB formation of high-angle boundaries during CRX of superplastic aluminum alloys, such as Supral 2004. Furthermore, the macro- and microtexture data as well as the disorientation results cannot be interpreted in terms of conventional models for development of superplastic microstructures in such alloys.[43,44,45] Finally, the DB model will be extended to interpret the response evolution of such a banded microstructure during deformation within the superplastic regime.

II. GRAIN REFINEMENT, GRAIN BOUNDARIES, AND SUPERPLASTICITY

From the perspective of applied mechanics, a material may exhibit superplasticity due to a high value of m, the strain-rate sensitivity coefficient of the flow stress, during plastic deformation. In fine-grained metals, this may arise during deformation under temperature and strain-rate conditions where grain-boundary sliding (GBS) is dominant during deformation. The GBS must be accommodated by either slip or stress-directed diffusion, and together, these processes constitute the mechanism for superplasticity. For this, grains must be equiaxed and highly refined with mobile grain boundaries that can slide while resisting tensile separation.[4,43,46]

A constitutive law that includes the independent, additive contributions of the superplastic and dislocation creep mechanisms may be used to describe the mechanical response of fine-grained superplastic metals.[43,46] Thus,

$$\dot{\varepsilon}_{\text{total}} = \dot{\varepsilon}_{sp} + \dot{\varepsilon}_{\text{disl}} \qquad [1]$$

where $\dot{\varepsilon}_{\text{total}}$ is the observed total strain rate, and $\dot{\varepsilon}_{sp}$ and $\varepsilon_{\text{disl}}$ are the contributions of the superplastic and dislocation creep mechanisms, respectively. The GBS and its accommodation mechanisms are envisioned to occur in grain boundaries and adjacent, mantlelike regions of the grains; accordingly, $\dot{\varepsilon}_{sp}$ is strongly dependent on grain size. Dislocation creep is usually presumed to occur independently in the core regions of the grains, and so, $\dot{\varepsilon}_{\text{disl}}$ is unaffected by changes in grain size. Various phenomenological constitutive relationships have been used to describe these mechanisms.[43,46] Here, two of them are combined to give

$$\dot{\varepsilon}_{\text{total}} = AD^*_{\text{eff}} \left(\frac{1}{\bar{L}}\right)^2 \left(\frac{\sigma}{E}\right)^2 + KD \left(\frac{\sigma}{E}\right)^N \qquad [2]$$

where A is a material constant for the superplastic mechanism, D^*_{eff} is a modified effective diffusion coefficient, $\bar{L}$ is the mean linear-intercept grain size, σ is the applied stress, and E is Young's modulus; K is a material constant for dislocation creep, and D and N are the appropriate diffusion coefficient and stress exponent for the dislocation creep mechanism. Depending on the specific dislocation creep mechanism, the stress exponent, N, may have values ranging from 3 to 5.

Equation [2] predicts a grain-size-dependent transition from dislocation creep at high values of the modulus-compensated stress, (σ/E), to slip- or diffusion-accommodated GBS at low values of (σ/E). If $D^*_{\text{eff}} \approx D_l$, the lattice diffusivity, and $N = 5$, *i.e.*, for dislocation climb-controlled creep, then Eq. [2] may be plotted as diffusion-compensated rate, $(\dot{\varepsilon}/D_l)$, *vs* (σ/E); for independent mechanisms, the fastest will be rate controlling. Using pure aluminum data (*e.g.*, Reference 2), Eq. [2] may be plotted for different values of the mean linear-intercept grain size; plots for $\bar{L} = 5\ \mu$m and $\bar{L} = 12\ \mu$m are shown in Figure 1. These grain size values are typical of those achieved through TMP in wrought superplastic aluminum alloys. For either grain-size value, there is a transition in the apparent stress dependence of the strain rate, from $n \approx 5$ to $n \approx 2$ as (σ/E) decrease, where $n \equiv d \log\left(\frac{\dot{\varepsilon}}{D_l}\right)/d \log\left(\frac{\sigma}{E}\right)$. Since $m \equiv (1/n)$, the strain-rate sensitivity coefficient increases from about 0.2 to 0.5 through this transition; the latter value is generally regarded as sufficient to support extensive superplastic response. It is clear in Figure 1 that a decrease in grain size increases the strain-rate range for superplastic response, and this is the basis for the requirement that $\bar{L} \leq 15\ \mu$m for useful superplasticity in engineering alloys.

High-angle grain boundaries are also a requirement for

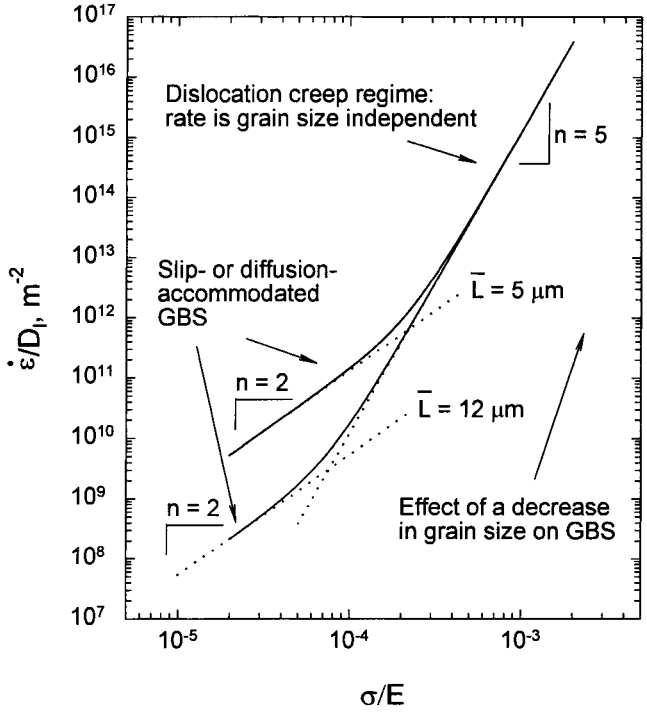

Fig. 1—Lattice-diffusion compensated strain rate as a function of the modulus-compensated stress for additive, independent dislocation creep and GBS mechanisms. The GBS mechanism is shown for two different grain sizes. The refinement of grain size results in an increased range of strain rates for useful superplastic response.

superplasticity. It is usually asserted that a fine, cellular dislocation or subgrain structure will not exhibit superplastic behavior because the lattice registry associated with low-angle boundaries precludes GBS.[43] However, little work has been reported on the relationship between grain-boundary characteristics, such as the distribution of boundary disorientation angles, and GBS in polycrystalline metals. One investigation of grain-boundary shear in aluminum tricrystals revealed that boundaries of 3 or 4-deg lattice rotation about a ⟨110⟩ axis did not slide at 600 °C. However, boundaries of 7-deg lattice rotation, or more, did slide at this temperature. Furthermore, the extent of sliding increased as the lattice rotation angle increased.[47]

Several mechanisms have been proposed to explain the formation of high-angle boundaries during CRX. These mechanisms usually consider that the TMP results in storage of dislocations in elongated prior grains and that subgrains of low disorientation form in the initial stages of annealing or elevated temperature deformation. A subsequent increase in boundary disorientation then follows due to subgrain growth,[48] subgrain coalesence,[49] subgrain rotation,[50] subgrain rotation and switching,[51] or accumulation of dislocations into subgrain boundaries.[52] More recent investigations[53] have shown that boundaries of relatively large disorientation may form as a result of grain subdivision processes during TMP of pure metals. However, the role of such boundaries, which formed as a result of prior deformation, in subsequent deformation processes, such as GBS, has not been determined. Also, there have been few investigations into the mechanisms of formation and evolution of boundaries in alloys that exhibit continuous recrystallization and into the role of such mechanisms in determining subsequent superplastic response. In one study, the effects of TMP parameters on CRX and the superplastic response of an Al-Mg-Zr alloy were examined. It was observed that the peak superplastic ductility increased dramatically when changes in the TMP parameters resulted in an increase in the population of 5 to 15 deg boundaries in the disorientation distribution.[54] The aim of the present investigation is to elucidate the mechanism of high-angle boundary formation in an aluminum alloy that exhibits CRX.

III. EXPERIMENTAL PROCEDURES

Supral 2004 material was obtained as a 2-mm sheet in the as-processed condition from Superform-USA, Inc. Riverside, CA. This material has been the subject of previous investigations, and details of the TMP have already been provided.[8,9,55] The alloy composition (in wt. pct) is provided in Table I. Tensile coupons with a gage length of 12.5 mm were machined from the as-rolled sheet such that the tensile axis was parallel to the final cold rolling direction (RD) of the sheet. Tension tests were performed at a constant strain rate of $10^{-2}\ s^{-1}$ at 450 °C, ensuring superplastic deformation.

Macrotexture measurements were carried out by means of the Schultz reflection method using a diffractometer equipped with closed Eulerian cradle. The (111), (200), (211), and (311) pole figures were obtained. The polar angle ranged from 0 to 90 deg in steps of 3 deg. From the pole figures, the even part of the three-dimensional orientation distribution function (ODF) of the Euler angles φ_1, Φ, and φ_2 was calculated by a series expansion method. Sample preparation consisted of grinding on successively finer silicon carbide papers and final mechanical polishing with 1-μm diamond paste.

Sample preparation for OIM consisted of grinding on successively finer silicon carbide papers (1000, 2400, and 4000 grits) followed by mechanical polishing with diamond grit sizes of 3 and 1 μm and finishing with 0.05 μm colloidal silica. The final electropolishing was conducted at 35 V for 20 seconds and employed a perchloric acid (20 pct)-ethanol (80 pct) solution cooled to an initial temperature of −25 °C.

Microtexture measurements were performed using electron backscatter diffraction (EBSD) methods and OIM. A thorough introduction to EBSD and OIM has been given by Randle.[56] The electron beam of a scanning electron microscope (SEM), operating in the spot mode, is used as a local orientation probe in OIM on samples of bulk material. System software and hardware (TSL Inc., Draper UT, subsidary of EDAX Inc., Mahway, NJ) was installed on a Topcon SM-510 SEM. Electron interactions within approximately 50 nm of the sample surface produce Kikuchi patterns on a phosphor screen in the SEM sample chamber. A low-light camera allows these patterns to be captured, analyzed, and unambiguously indexed in terms of the Euler angles, ϕ_1, Φ, and ϕ_2, which describe the local lattice orientation relative to the sample axes. The electron beam is deflected, point-by-point, in a raster pattern on the sample surface, and the orientation data are acquired and stored along with the location of each point on the sample surface. The point-to-point step size was based on the expected microstructure and size of the region being examined. Data cleanup procedures were employed to ensure that data points with a probability >95 pct of correct indexing were retained in the analysis. Individual points having lower probability of correct indexing were

Table I. Alloy Composition (Weight Percent) for the As-Received SUPRAL 2004

	Cu	Zr	Fe	Si	Zn	Mn	Mg	Ti	Li	Al
Cast number 2004F013	5.66	0.37	0.14	0.06	0.029	0.013	0.003	0.005	0.0001	bal

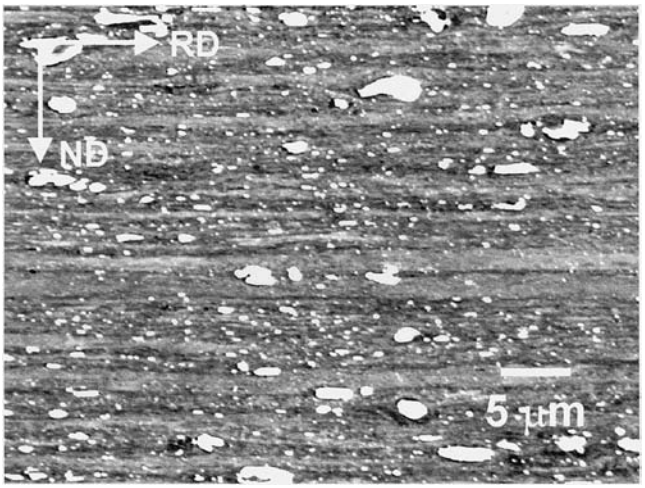

Fig. 2—The microstructure of as-processed Supral 2004 in the RN plane consists of elongated, banded features. Backscatter electron image, orientation contrast, and no etchant.

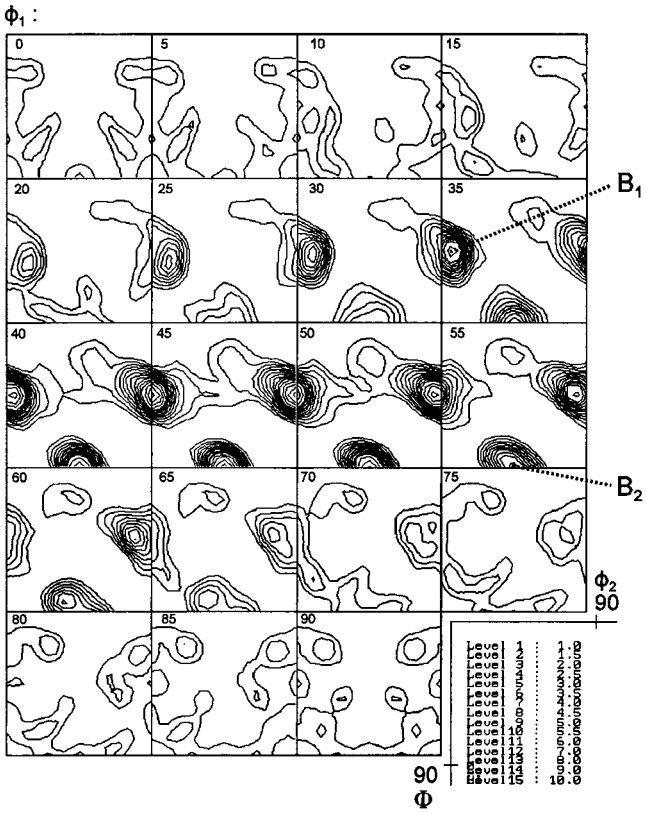

Fig. 3—Texture data for as-processed Supral 2004 in the form of the X-ray ODF. A deformation texture that has a predominant B component is apparent; the two variants of the B texture component are indicated (refer to the text).

reassigned to neighboring regions of similar orientation. This method was chosen to reduce the effects of pattern overlap or loss of pattern sharpness in the vicinity of grain boundaries and second-phase particles. The production of grain maps based on the orientation measurements was accomplished by assigning points (pixels) to a grain in regions with neighboring orientations differing by less than 2 deg. The orientation data may also be represented by assigning gray tones to pixels based on quality (sharpness) of the Kikuchi pattern image. Finally, the orientations may also be plotted as discrete pole figures as representations of the microtexture in the regions of the maps. Highlighting functions in the software were employed to correlate local lattice orientation as reflected in pole figures to the location of the orientation in the microstructure. This same feature may also be employed to determine the locations of the high (50 to 62.8 deg) and low (2 to 15 deg) angle boundaries on the grain maps.

IV. RESULTS

A. *Effect of Annealing on As-Processed Supral 2004*

Figure 2 is a backscattered electron micrograph illustrating the as-received microstructure of this material. This micrograph reflects the severe cold deformation of the final stage of the TMP[8,9,55] and shows the formation of highly elongated, bandlike features aligned with the RD. A coarse dispersion of $\theta(Al_2Cu)$ particles, which range in size from 0.5 to 4 μm, is also evident. The particles also tend to be elongated in the RD.

Macrotexture data for the as-received condition are shown in Figure 3 in the form of φ_1 = constant sections of the X-ray ODF. Relative intensity contours, beginning with 1 and increasing in intervals of 0.5, have been used in order to facilitate comparison among the different conditions. The orientations lay mainly along the α fiber but are not uniformly distributed along it. Instead, the orientations are grouped in two regions, which correspond to the Euler angles {φ_1 = 25 to 45 deg; Φ = 45 deg; φ_2 = 0 deg} and {φ_1 = 45 to 65 deg; Φ = 90 deg; φ_2 = 45 deg}. It is important to note that the two symmetric variants of the B-texture component, which are {φ_1 = 35 deg; Φ = 45 deg; φ_2 = 0 deg} (B_1); and {φ_1 = 55 deg; Φ = 90 deg; φ_2 = 45 deg} (B_2), lay approximately at the centers of these distributions along the α fiber. Thus, the texture of this as-received Supral 2004 exhibits a B-type deformation texture that is spread along the α fiber.

The microstructure and macrotexture data are consistent with the OIM results presented in Figure 4. In the OIM grain map of Figure 4(a), randomly selected colors are assigned to regions in which the orientation differs by less than 2 deg, and a gray scale representing Kikuchi pattern image quality is then superimposed. Low image quality is indicated by the darker gray tones. These data show elongated grains that are aligned with the RD, while low image quality near boundaries and in regions between the grains reflects lattice distortion due the TMP.

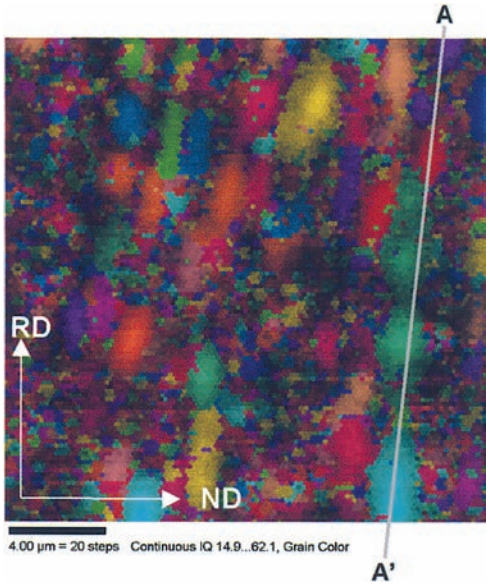

(*a*)

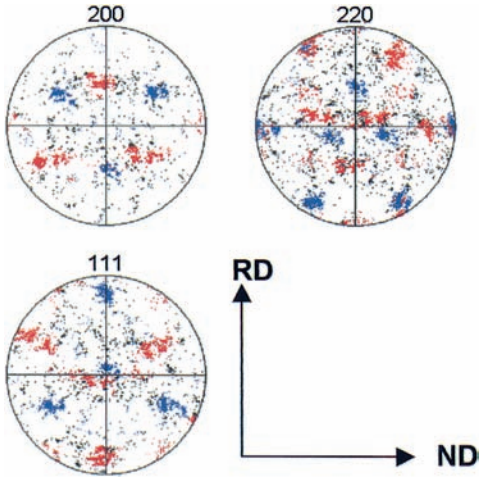

(*b*)

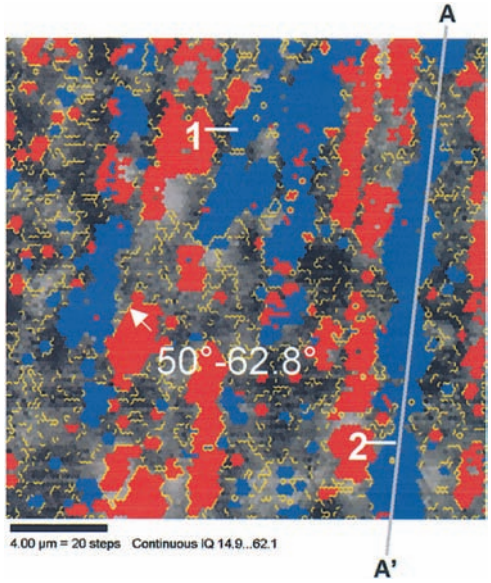

(*c*)

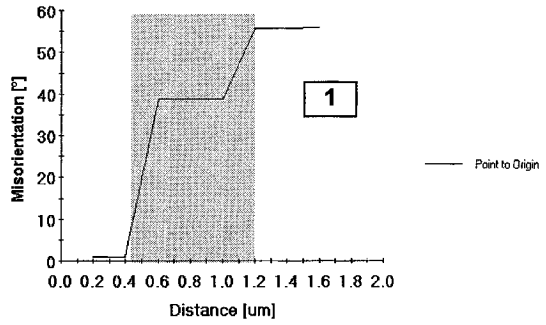

(*d*)

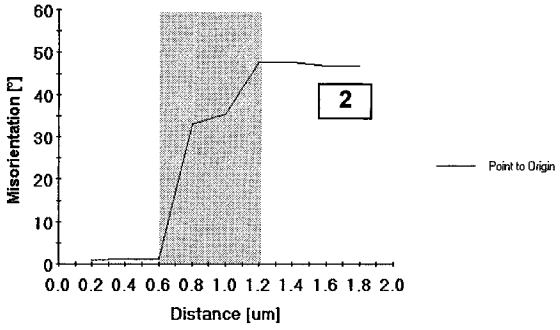

(*e*)

Fig. 4—(*a*) An OIM unique grain color map, wherein neighboring points of disorientation <2 deg are assigned the same grain color, with superimposed image quality. (*b*) Discrete pole figures, with the symmetric variants of the B texture component highlighted in either red or blue. (*c*) An image for the same data as in (*a*), except that orientations within 15 deg of each symmetric variant of the texture are highlighted in either red or blue. The lines denoted A-A′ in (*a*) and (*c*) delineate the position of a band of lattice orientation corresponding to one of the symmetric variants of the texture. (*d*) and (*e*) Linear traverses through the microstructure along the indicated lines show gradual transitions in lattice orientation from one variant orientation to the next.

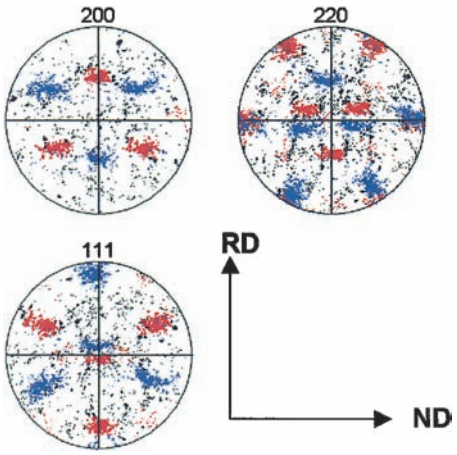

(*a*)

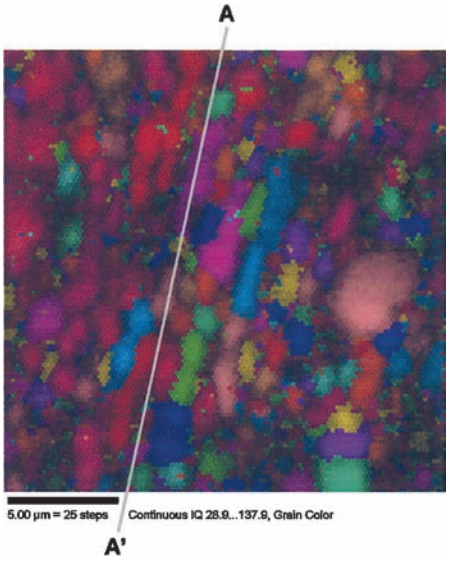

(*b*)

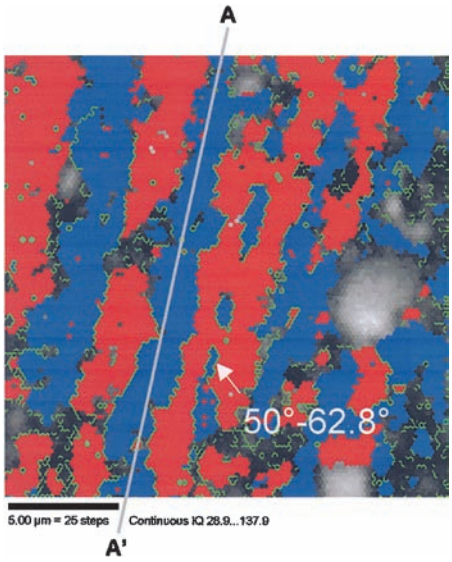

(*c*)

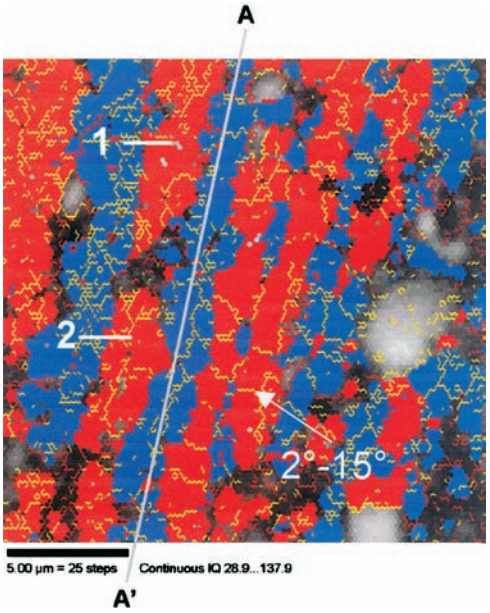

(*d*)

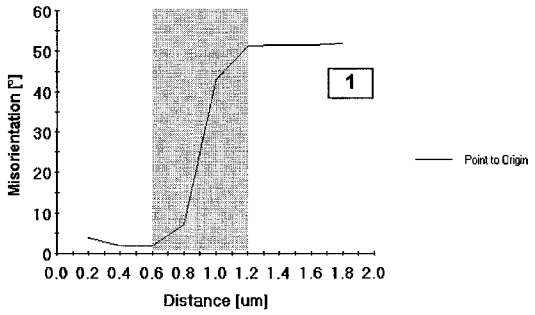

(*e*)

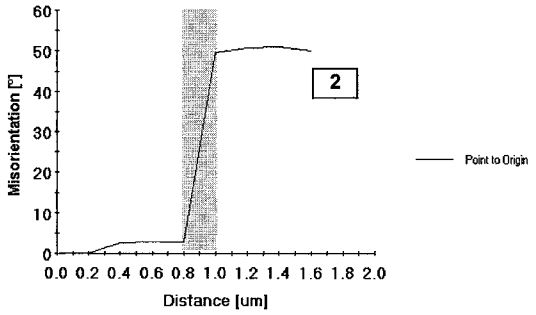

(*f*)

Fig. 5—OIM data for Supral 2004 after 6 h of annealing at 450 °C. (*a*) Discrete pole figures indicating retention and sharpening of the texture. (*b*) A unique grain color map showing a distinct grain structure. (*c*) An image for the same data as in (b), except that orientations within 15 deg of each texture variant have been highlighted in either red or blue. This reveals that the structure consists of alternating bands of lattice orientation that correspond to the B_1 and B_2 variants of the texture. The lines denoted A-A′ in (*b*) through (*d*) delineate the position of a band of lattice orientation corresponding to one of the symmetric variants of the texture. The high-angle boundaries are the interfaces between the bands, while the low-angle boundaries separate cells within the bands. The transition regions show more abrupt lattice orientation changes after annealing in (*e*) and (*f*).

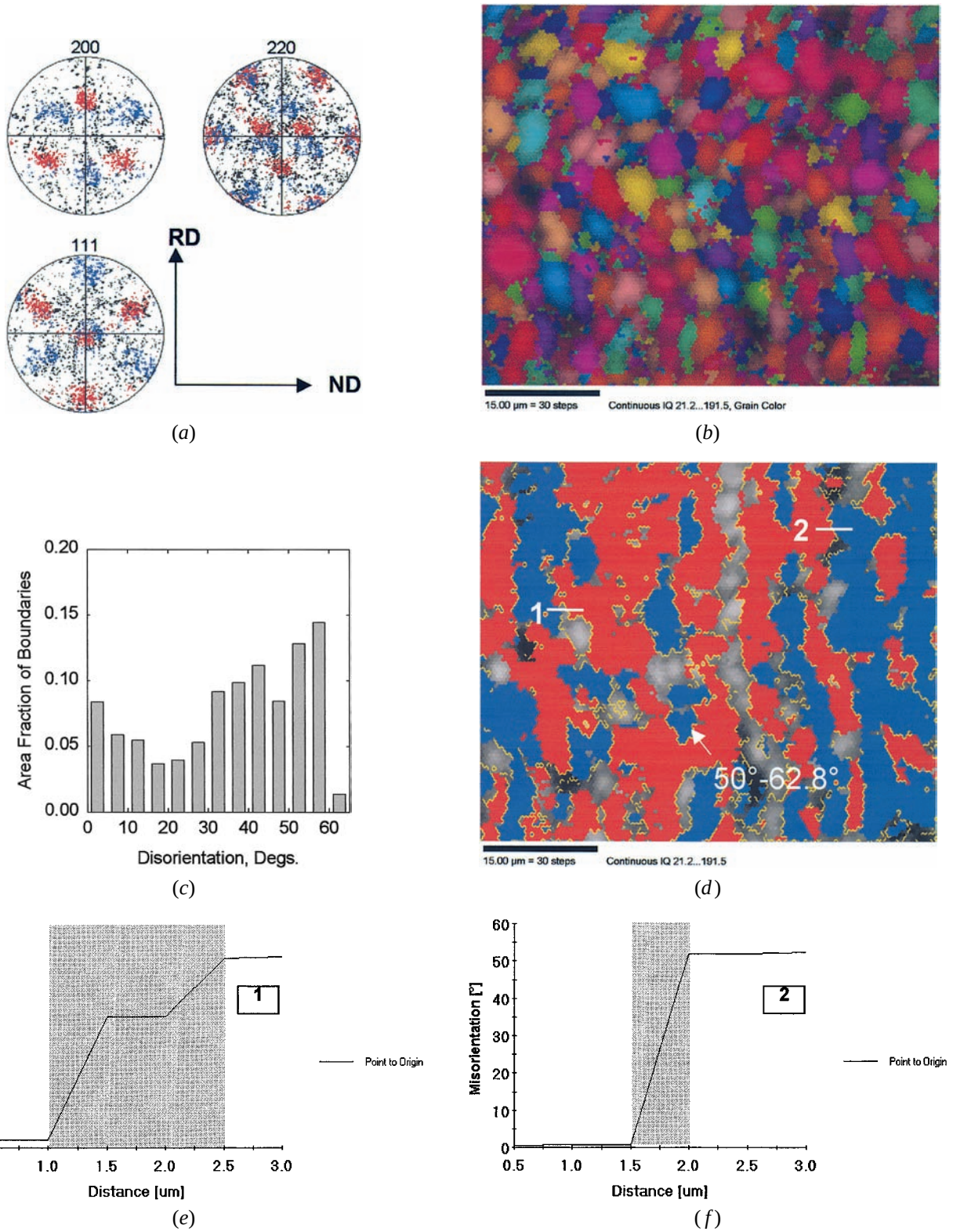

Fig. 6—(*a*) The discrete pole figures for material deformed to an elongation of 110 pct at 450 °C and 10^{-2} s^{-2} show that the B texture component is retained. (*b*) A unique grain color map showing a fine grain structure. (*c*) A bimodal disorientation distribution, with a low-angle peak corresponding to a cell structure within the bands and (*d*) high-angle boundaries that are interfaces between the bands. (*e*) and (*f*) Transitions from one band orientation to the next, which are again gradual.

Discrete pole figures are shown in Figure 4(b) for the as-received material, and they include all orientations having a confidence level >95 pct of correct Kikuchi pattern indexing. A B-type texture is apparent. Orientation determination in OIM is unambiguous, and so the two variants of the B texture, which are $(110)[1\bar{1}2]$ and $(011)[2\bar{1}1]$, may be

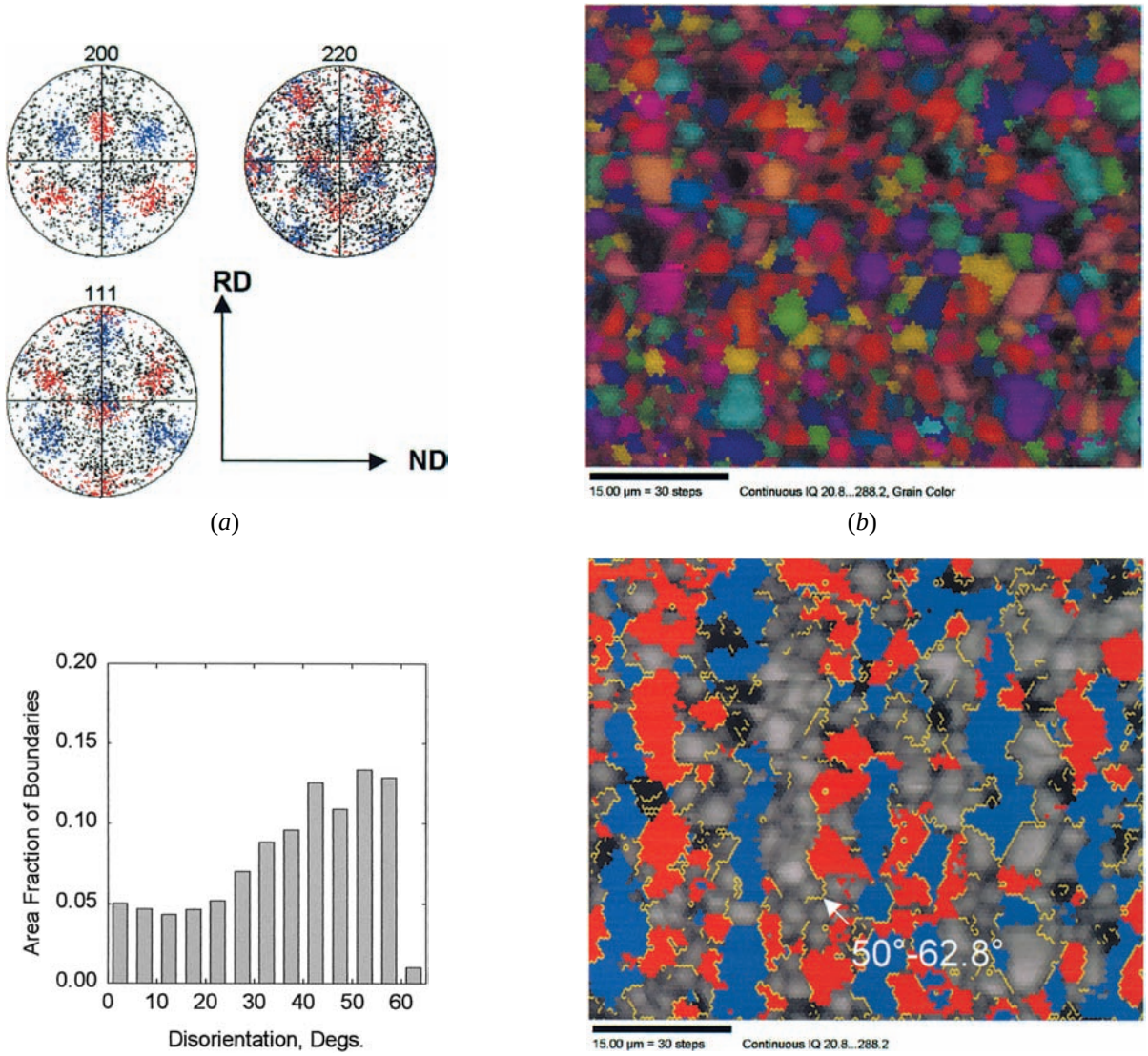

Fig. 7—(*a*) Discrete pole figures for material deformed 200 pct at 450 °C and 10^{-2} s^{-1} show weakening of the B texture component due to the onset of GBS. (*b*) The refined grain size (3 μm) apparent in this unique grain color map accounts for high superplastic ductility in this material. (*c*) Random disorientations become apparent in the disorientation distribution, while (*d*) the band structure is beginning to break up due to the onset of GBS.

distinguished in the data. This is accomplished by highlighting all orientations that lay within 15 deg of either variant in either red or blue, respectively, as indicated in Figure 4(b).

In OIM, the data acquired at each point includes the location corresponding to each individual orientation. Thus, the grain map of Figure 4(a) may also be color coded to indicate the locations of orientations corresponding to the two variants of the texture. This is shown in Figure 4(c); image quality (gray tones) alone is used for points corresponding to orientations that lay more than 15 deg from either variant. These data show that the microstructure is composed of elongated, bandlike regions about 2.5 μm in thickness that are aligned with the RD. Interspersed between these bands are regions of more nearly random orientation. The lattice orientation within the bands alternates along the normal direction (ND) between the orientations of the two variants of the main, B-texture component. Boundaries can also be identified in the data, and the yellow lines in Figure 4(c) reveal disorientations of 50 to 62.8 deg between adjacent pixels in the image. In some locations, the bands are immediately adjacent to one another, and at the resolution of OIM (0.2 μm), these are high-angle boundaries. Elsewhere in the image, there appear to be transition regions between the bands. Linear traverses were obtained along the ND in two such locations, as indicated on Figure 4(c). In each case, the lattice reorientation, or misorientation, relative to the origin of the traverse, may be plotted as a function of distance along the traverse. The results of these analyses are shown in Figures 4(d) and (e); in both cases, lattice rotation from the orientation of one variant to that of the other takes place through a transition region that is 0.6 to 0.8 μm in extent along the ND. While the transition appears to occur in steps, the data were acquired at the limit of resolution of the OIM technique, precluding definite conclusions about the character of the transition region.

Results of OIM analysis for a sample annealed 6 hours at 450 °C are shown in Figure 5. The microtexture data

(Figure 5(a)) show that the deformation texture of the as-processed material has remained stable during this annealing treatment, and no new components have appeared. A fine, uniform (sub)structure, with less lattice strain and having a 2 to 2.1-μm mean linear intercept, has become apparent in the grain color image of Figure 5(b). Following annealing, the band structure observed in the as-received material has become more sharply defined, as shown in Figure 5(c). The effect of annealing appears to be the thickening of the bands at the expense of the transition regions that separated them in as-received material; the bands are now 3 to 4 μm in thickness (Figure 4(c)). Following annealing, interfaces between the bands appear to extend more or less continuously in the RD, and at the resolution of OIM, these interfaces correspond to boundaries of 50 to 62.8 deg disorientation. These boundaries are highlighted in green in Figure 5(c), while the locations of boundaries of 2 to 15 deg disorientation are highlighted in yellow in Figure 5(d). Two representative examples of linear traverses along the ND through this band structure are shown in Figures 5(e) and (f). In general, the transition regions have become thinner; often, the transition takes place in one pixel (0.2 μm), as shown in Figure 5(e) although transition regions up to 0.6 μm in thickness may still be found in the microstructure (Figure 5(f)).

B. *Microstructural Evolution during Superplastic Deformation*

The results of OIM analysis for a sample deformed in tension to a strain of 110 pct are shown in Figure 6, while data for a sample deformed to a strain of 200 pct are shown in Figure 7. These samples were deformed at $T = 450$ °C and a nominal strain rate of 10^{-2} s^{-1}, *i.e.*, optimum superplastic conditions wherein the ductility was approximate 1000 pct elongation to failure. The B texture is clearly retained after 110 pct elongation under these conditions (Figure 6(a)), although it is not as sharp as in annealed material. The total time at temperature is approximately 45 minutes for this sample, which is much less than the annealing time for the data of Figure 5. Thus, it is apparent in the grain color image of Figure 6(b) that strain-enhanced grain growth has taken place, and a mean linear-intercept grain size of about 5 μm is apparent. It is important to note that the step size between orientation measurements (and pixels) is 0.5 μm for these data. Bimodal distributions of grain-to-grain disorientation angles have been presented in previous work.[7,8,9,54,55] The population of boundaries of 2 to 5 deg disorientation in Figure 6(c) is larger than that reported previously for this material, but otherwise, these data are consistent with the previous work on it.[8,9,55] The high-angle boundaries in the disorientation distribution are still predominantly the interfaces between bands of lattice orientation corresponding to the symmetric variants of the B-texture component, as shown in Figure 6(d). The regions shown in gray tones are more prominent than in material that has been annealed but not deformed, and they have lattice orientations in the random population. This likely reflects lattice (grain) rotation associated with GBS. Transition regions between bands now appear to thicken with deformation and have reached widths along the ND of 1.5 μm (Figure 6(e)), although elsewhere in the microstructure the reorientation from one band to the next takes place within one pixel in the image (Figure 6(f)).

At a strain of 200 pct, the microtexture still shows a B component, although the population of random orientations is clearly larger than in the data for material deformed to only 110 pct. No grain elongation is apparent in Figure 7(b). The mean linear-intercept grain size is about 3 μm after 200 pct elongation, which indicates grain refinement after an initial interval of strain-enhanced grain coarsening, and the disorientation distribution data (Figure 7(c)) suggest an increasing population of random boundaries in the distribution of grain-to-grain disorientations. The high-angle (50 to 62.8 deg) boundaries are still predominately interfaces between the bands. The band structure evident in annealed material (Figure 5(c)), which was prominent in material deformed 110 pct (Figure 6(d)), is still discernable after 200 pct elongation. However, the elongated character of the bands is giving way to individual grain clusters that are aligned with the RD and interspersed with grains of random orientation. Altogether, these results are consistent with the gradual onset of GBS over a large interval of strain under these conditions.

V. DISCUSSION

Superplasticity requires both a fine, stable grain structure and high-angle boundaries for GBS and its accommodation mechanisms, and TMPs involving large strain deformation and recrystallization are necessary in order to realize such microstructural features and enable superplasticity in aluminum alloys. The phenomenon of CRX apparently provides the necessary microstructures and results in highly superplastic response in alloys, such as Supral 2004. However, the mechanisms involved in this phenomenon have remained unclear and approaches to achieve and control CRX have been mainly empirical in nature. The OIM data of this research have illustrated the importance of a particular mechanism, DB, in grain refinement and development of high-angle boundaries in association with CRX after TMP.

A. *Deformation Banding in the As-Rolled Material*

The as-rolled Supral 2004 exhibits an elongated and banded microstructure and a deformation texture with a predominant B component; such a texture is characteristic of fcc metals deformed by rolling at low temperatures. The microtexture data for the as-received material are consistent with the X-ray data, and furthermore, bandlike features are apparent in the OIM data. Within a tolerance of 15 deg, the lattice orientation of the bands alternates along the ND according to the pattern, B_1, B_2, B_1, B_2, . . . , where B_1 would be $(110)[1\bar{1}2]$ and B_2 is $(011)[2\bar{1}1]$, in traverses along the ND on the RD/ND plane. Here, B_1 and B_2 refer to the symmetric variants of the B-texture component.

Figure 8 is a schematic illustration of the shape change associated with plane-strain deformation and the development of the B-texture component. This schematic is based on the analysis of Hirsch and Lücke[57] and also illustrates the crystallography of the two distinct variants of the B-texture component. A cube of fcc material having a B-type lattice orientation may deform on only two slip systems under a Tucker-type of stress state ($\sigma_{ND,ND} = \sigma_{RD,RD}$) and,

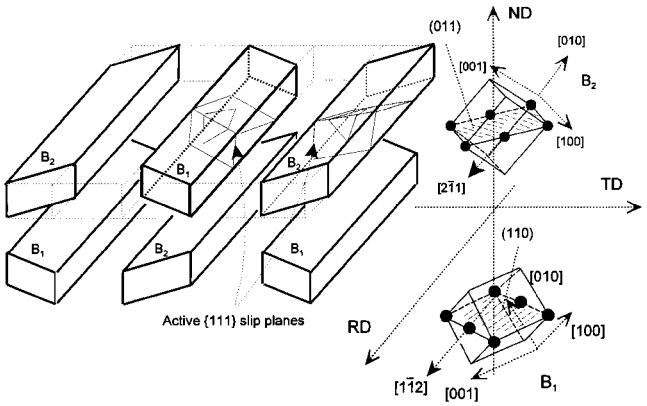

Fig. 8—A schematic representation shows a structure consisting of alternating variants of the B texture component. Arranging the variants in an alternating fashion allows macroscopic plane strain deformation for the aggregate.

except for an additional shear strain, $\varepsilon_{RD,ND}$, exhibit plane strain deformation ($\varepsilon_{ND,ND} = -\varepsilon_{RD,RD}$; $\varepsilon_{TD,TD} = 0$). The sense of the shear strain, $\varepsilon_{RD,ND}$, is equal but opposite for the B_1 and B_2 variants, as illustrated in Figure 8. Thus, by arranging deformed and elongated regions having the B_1 an B_2 variant orientations in an alternating pattern, as shown in Figure 8, the shear terms average out, and a region having such a pattern may deform macroscopically in plane strain.

Grain subdivision, with lattice rotation toward the B_1 variant orientation on one side of a developing boundary and the B_2 variant orientation on the opposite side of the boundary, would lead eventually to the microstructure illustrated in the OIM data of Figure 4. Thus, a DB model for the deformation microstructure of Supral 2004 includes grain subdivision during the prior TMP with the development of bands of lattice orientations that alternate between the symmetric variants of the deformation texture. The bands that are apparent in Figure 4 are about 2.5 μm in thickness, which is approximately the thickness expected if prior grains that are initially 50 μm in size prior to rolling are reduced by a true strain of 3. However, investigations into DB have generally shown that the process of grain subdivision begins at much smaller strains and involves formation of several bands within each prior grain.[13–18] The prior boundaries are indistinguishable in either of Figures 2 or 4, and so it would be necessary to examine the evolution of DB during rolling in order to assess the interaction between the bands and the prior grains.

Following annealing, the bands have a thickness-to-length aspect ratio of 10:1, or more, and an equiaxed cellular structure, comprising many boundaries of 2 to 15 deg disorientation, has become apparent within the bands (Figure 5(d)). The cells appear to be 1 to 2 μm in size. Thus, from one to three cells are encountered in a traverse along the ND across each band. The presence of the Al_2Cu particles and the shear strain, $\varepsilon_{RD,ND}$, at the ends of the bands must be accommodated by additional local strains within the bands. These accommodation strains account for the presence of the cellular substructure within the bands. The large apparent disorientations associated with the cell walls reflect a high dislocation density developed during TMP as well as low rates of recovery due to the high solute content and presence

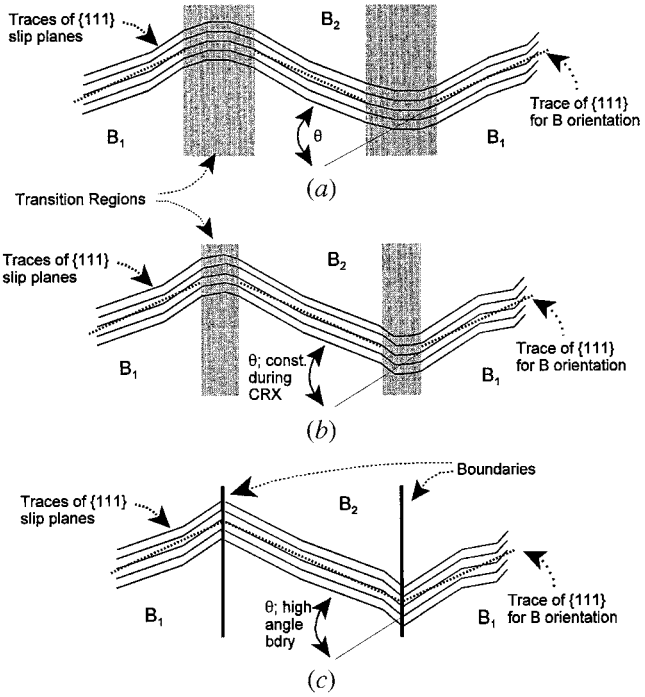

Fig. 9—A schematic representation of the formation of boundaries from transition regions separating adjacent bands of lattice orientation corresponding to the two variants of the B component. (*a*) Bands are thick regions through which lattice orientation varies from that of one variant to that of the next. (*b*) During annealing, recovery results in elimination of cells within the transition regions and they become thinner. (*c*) Eventually, high-angle boundaries evolve from such regions.

of the Al_3Zr particles. The main B-texture component reflects DB during the prior TMP of the material, while the presence of a cellular substructure due to accommodation accounts for the spread about the B-texture component.

B. *Superplastic Deformation of a Banded Microstructure*

The disorientations immediately after TMP correspond to features of the deformation microstructure, including interfaces between bands and a cellular structure within the bands. The presence of transition regions, wherein lattice orientation changes gradually from one band orientation to the next, suggests that the band/band interfaces are extended regions of high dislocation density rather than distinct boundaries. The details of such regions require higher spatial resolution than attainable in OIM. A schematic representation of the effect of annealing is suggested in Figure 9. The thick, shaded regions represent the transition regions between bands or cells in the deformation microstructure. Reorientation of the lattice from one band or cell to the next takes place gradually through the transition region (Figure 9(a)). The effect of annealing is suggested in Figures 9(b) and (c). Thus, recovery-controlled rearrangement of dislocation structures and processes, such as cell wall or subgrain boundary coalescence within a transition region, allows the band or cell to grow at the expense of the transition region. The lattice orientation within the bands or cells on either side of such an evolving structure is envisioned to be unaffected during such a process, which is consistent with the stability

of the texture. Eventually, the transition regions are replaced by distinct boundaries.

The OIM results (Figures 6 and 7) suggest that the processes of boundary development from these transition regions occur progressively at 450 °C with concurrent straining under superplastic conditions. The retention of the B-texture component as well as the band structure after a strain of 110 pct suggests that few boundaries have become able to slide at this point, and so deformation is predominately by dislocation creep processes despite the apparent fineness of the grain structure. Under dislocation creep conditions, a distinct ⟨111⟩ fiber texture formed during deformation of a 5083 alloy, which had a fine, recrystallized grain size and a random initial texture after TMP to make this material superplastic.[2] Examination of the discrete (111) pole figure in Figure 6(a) reveals that a ⟨111⟩ is nearly aligned with the RD, which is also the tensile axis, in both the B_1 and B_2 variants of texture. Thus, only small lattice rotations would be required during uniaxial tensile extension along RD, and this is reflected in the apparent stability of this orientation here.

At a strain of 200 pct, the randomizing of the texture and grain-boundary disorientation distribution suggest that boundary development from the band and cell boundaries is essentially complete, and GBS is now contributing a large proportion of the total superplastic strain. A mean linear-intercept grain size of 3 μm allows superplastic response over a wide strain-rate range. Comparison of the disorientation distributions in Figures 6(c) and 7(c) shows that the populations of low-angle (2 to 5 deg) and high-angle (50 to 62.8 deg) are decreasing. However, a peak at 40 to 45 deg in the disorientation histogram of Figure 7(c) is in the same range as predicted by Mackenzie for randomly oriented cubes,[58] and this is consistent with the random grain rotations associated with GBS.

In summary, the retention and sharpening of the texture and the appearance of a fine grain structure in the absence of high-angle boundary migration are consistent with CRX. Previously proposed mechanisms for this process[48–52] are not fully consistent with the OIM results of the present work. Instead, DB during the severe deformation of the prior TMP results in a banded microstructure. The process of high-angle boundary formation takes place gradually throughout TMP and subsequent annealing or elevated temperature deformation. The high-angle boundaries do not form as a result of random processes; rather, they separate bands having lattice orientations corresponding to the symmetric variants of the main, B-type texture component.

Transition regions between bands of alternating lattice orientation, as well as within the bands, account for lattice reorientation but initially are not distinct boundaries. Boundaries evolve gradually during annealing or during deformation at elevated temperature from such transition regions. The alteration of the diffuse dislocation structures of these transition regions and their relaxation to form high-angle boundaries have been described previously.[52] These processes occur while the disorientation across the transition region remains essentially constant (and texture does not vary) while the boundary develops. Thus, the formation of distinct boundaries from such transition regions in a banded microstructure constitutes the phenomenon of CRX in Supral 2004.

VI. CONCLUSIONS

The observations of this work constitute direct experimental evidence for DB in the development of microstructure during TMP of this material. The DB model has been previously proposed to explain the evolution of macro- and micro-texture of this alloy[54] but not based on direct observation of the structure. The band structure is retained during annealing and persists during elevated temperature deformation even under conditions of optimum superplastic response for this aluminum alloy. Control of DB formation during TMP may facilitate control of the development of high-angle boundaries in support of improved superplastic response of such materials.

Continuous recrystallization during static annealing consists of recovery-controlled formation of boundaries from transition regions between bands and between the cells of a cellular dislocation structure within the bands. The formation of boundaries by the recovery-controlled sharpening of the band interfaces and cell walls accounts for the retention and sharpening of the deformation texture as the volume fraction of material associated with transition regions decreases. At the initiation of elevated temperature deformation of such a banded microstructure, straining takes place with simultaneous contributions from dislocation creep and GBS. Even under conditions corresponding to optimum superplastic response, dislocation creep predominates at the beginning of the deformation while interfaces are evolving, and most of them are still not capable of sliding. Once a sufficient area fraction of high-angle boundaries are formed, GBS begins and becomes mainly responsible for the subsequent deformation process.

ACKNOWLEDGMENTS

The authors acknowledge Mr. A.J. Barnes, Superform-USA (Riverside, CA), for the provision of the Supral 2004 alloy of this research.

REFERENCES

1. R.D. Doherty, D.A. Hughes, F.J. Humphreys, J.J. Jonas, D. Juul Jensen, M.E. Kassner, W.E. King, T.R. McNelley, H.J. McQueen, and A.D. Rollett: *Mater. Sci. Eng.*, 1997, vol. A238, pp. 219-74.
2. M.T. Pérez-Prado, G. González-Doncel, O.A. Ruano, and T.R. McNelley: *Acta Mater.*, 2001, vol. 49, pp. 2259-68.
3. M.T. Pérez-Prado, T.R. McNelley, G. González-Doncel, and O.A. Ruano: Naval Postgraduate School, Monterey, CA, unpublished research, 2001.
4. R. Grimes: in *Superplasticity*, Lecture Series 168, NATO Advisory Group for Aerospace Research and Development (AGARD), Paris, 1988, pp. 8.1–8.16.
5. B.M. Watts, M.J. Stowell, B.L. Baike, and D.G.E. Owen: *Met. Sci. J.*, 1976, vol. 10 (6), pp. 189-97.
6. F.J. Humphreys: *Acta Mater.*, 1997, vol. 45, pp. 4231-40.
7. M.T. Pérez-Prado, T.R. McNelley, O.A. Ruano, and G. González-Doncel: *Metall. Mater. Trans. A*, 1998, vol. 29A, pp. 485-92.
8. T.R. McNelley and M.E. McMahon: *Metall. Mater. Trans. A*, 1997, vol. 28A, pp. 1879-87.
9. T.R. McNelley, M.E. McMahon, and M.T. Pérez-Prado: *Phil. Trans. R. Soc. A*, 1999, vol. 357, pp. 1683-1705.
10. C.S. Barrett: *Trans. Am. Inst. Min. Eng.*, 1939, vol. 135, pp. 296-324.

11. C.S. Barrett and L.H. Levenson: *Trans. Am. Inst. Min. Eng.*, 1940, vol. 137, pp. 112-26.
12. G.Y. Chin and B.C. Wonsiewicz: *Trans. AIME*, 1969, vol. 245, pp. 871-72.
13. B.J. Duggan and C.S. Lee: *Scripa Metall. Mater.*, 1992, vol. 27, pp. 1503-07.
14. C.S. Lee, R.E. Smallman, and B.J. Duggan: *Mater. Sci. Technol.*, 1994, vol. 10, pp. 862-68.
15. C.S. Lee, B.J. Duggan, and R.E. Smallman: *Acta Metall. Mater.*, 1993, vol. 41, pp. 2265-70.
16. C.S. Lee and B.J. Duggan: *Acta Metall. Mater.*, 1993, vol. 41, pp. 2691-99.
17. C.S. Lee, B.J. Duggan, and R.E. Smallman: *J. Phys. IV*, 1993, vol. C7, p. 2027.
18. C.S. Lee, R.E. Smallman, and B.J. Duggan: *Scripta Metall. Mater.*, 1995, vol. 33, pp. 727-33.
19. J.R. Hirsch: *Mater. Sci. Technol.*, 1990, vol. 6, pp. 1048-57.
20. A. Godfrey, D. Juul Jensen, and N. Hansen: *Acta Mater.*, 1998, vol. 46 (3), pp. 823-33.
21. G.I. Taylor: *J. Inst. Met.*, 1938, vol. 63, pp. 307-24.
22. K. Kulkarni, E.A. Starke, Jr., and D. Kuhlmann-Wilsdorf: *Acta Mater.*, 1998, vol. 46, pp. 5283-5301.
23. J. Liu, M. Mato, and R.D. Doherty: *Scripta Metall.*, 1989, vol. 23, pp. 1811-16.
24. P. Cizek, B.A. Parker, and B.J. Wynne: *Scripta Metall. Mater.*, 1995, vol. 32, pp. 319-23.
25. P. Wagner, O. Engler, and K. Lücke: *Acta Metall. Mater.*, 1995, vol. 43, pp. 3799-3812.
26. S.P. Bellier and R.D. Doherty: *Acta Metall.*, 1977, vol. 25, pp. 521-38.
27. S. Li, B. Gong, and Z. Wang: *Scripta Metall. Mater.*, 1994, vol. 31, pp. 1729-34.
28. K. Kashihara, M. Tagami, and F. Inoko: *Mater Trans. JIM*, 1996, vol. 37, pp. 564-71.
29. K. Kashihara, M. Tagami, and F. Inoko: *Mater. Trans. JIM*, 1996, vol. 37, pp. 572-78.
30. B. Gong, Z. Wang, D. Chen, and Z. Wang: *Scripta Mater.*, 1997, vol. 37, pp. 1605-10.
31. Y. Inokuti and R.D. Doherty: *Acta Metall.*, 1978, vol. 26, pp. 61-80.
32. J.H. Driver, D. Juul Jensen, and N. Hansen: *Acta Metall. Mater.*, 1994, vol. 42, 3105-14.
33. T. Wang, B.L. Adams, and P.R. Morris: *Metall. Trans. A*, 1990, vol. 21A, pp. 2223-36.
34. F. Li and P.S. Bate: *Acta Metall. Mater.*, 1991, vol. 39, pp. 2639-50.
35. R. Becker, J.F. Butler, Jr., H. Hu, and L.A. Lalli: *Metall. Trans. A*, 1991, vol. 22A, pp. 45-58.
36. A. Akef and J.H. Driver: *Mater. Sci. Eng.*, 1991, vol. 132, pp. 245-55.
37. P. Cizek, B.P. Wynne, H. Lu, and B.A. Parker: *Mater. Sci. Eng.*, 1996, vol. 219, pp. 44-55.
38. Y. Inokuti, F. Saito, and C. Gotoh: *Mater. Trans. JIM*, 1996, vol. 37, pp. 203-09.
39. A. Korbel, J.D. Embury, M. Hatherly, P.L. Martin, and H.W. Erbsloh: *Acta Metall.*, 1986, vol. 34, pp. 1999-2009.
40. H. Hu: *Acta Metall.*, 1962, vol. 10, pp. 1112-16.
41. P. Bate and A. Oscarsson: *Mater. Sci. Technol.*, 1990, vol. 6, pp. 520-27.
42. B. Bay, N. Hansen, D.A. Hughes, and D. Kuhlmann-Wilsdorf: *Acta Metall. Mater.*, 1992, vol. 40, pp. 205-19.
43. T.G. Nieh, J. Wadsworth, and O.D. Sherby: in *Superplasticity in Metals and Ceramics*, D.R. Clarke, S. Suresh, and I.M. Ward, eds., Cambridge University Press, Cambridge, United Kingdom, 1997.
44. A.H. Chokshi, A.K. Mukherjee, and T.G. Langdon: *Mater. Sci. Eng. R*, 1993, vol. 10, pp. 237-74.
45. O.A. Kaibyshev: *Superplasticity of Alloys, Intermetallics and Ceramics*, Springer-Verlag, Berlin, 1992.
46. O.D. Sherby and J. Wadsworth: in *Deformation Processing and Microstructure*, G. Krauss, ed., ASM, Metals Park, OH, 1982, pp. 355-89.
47. F. Weinberg: *Trans. AIME*, 1958, vol. 212, pp. 808-17.
48. R. Orsund and E. Nes: *Scripta Metall.*, 1989, vol. 23 (7), pp. 1187-92.
49. E. Hornbogen: *Metall. Trans. A*, 1979, vol. 10, pp. 947-72.
50. H. Gudmundsson, D. Brooks, and J.A. Wert: *Acta Mater.*, 1991, vol. 39, pp. 19-35.
51. M.T. Lyttle and J.A. Wert: *J. Mater. Sci.*, 1994, vol. 29, pp. 3342-50.
52. S.J. Hales, T.R. McNelley, and H.J. McQueen: *Metall. Trans. A*, 1991, vol. 22A, pp. 1037-47.
53. D.A. Hughes and N. Hansen: *Acta Mater.*, 1997, vol. 45, pp. 3871-86.
54. T.R. McNelley and M.E. McMahon: *Metall. Mater. Trans. A*, 1996, vol. 28A, pp. 2252-62.
55. M. Eddahbi, T.R. McNelley, and O.A. Ruano: *Metall. Mater. Trans. A*, 2001, vol. 32A, pp. 1093-1102.
56. V. Randle: *Microtexture Determination and Its Applications*, The Institute of Metals, London, 1992.
57. J. Hirsch and K. Lücke: *Acta Metall.*, 1988, vol. 36, pp. 2883-2904.
58. J.K. MacKenzie: *Biometrica*, 1958, vol. 45, pp. 229-40.